Genetics in Medicine (2024) 26, 101143

ELSEVIER

Genetics in Medicine
An Official Journal of the ACMG

www.journals.elsevier.com/genetics-in-medicine

ARTICLE

Biallelic loss-of-function variants of *ZFTRAF1* cause neurodevelopmental disorder with microcephaly and hypotonia

Maria Asif[1,2], Arwa Ishaq A. Khayyat[3], Salem Alawbathani[1,4], Uzma Abdullah[5], Anne Sanner[6], Theodoros Georgomanolis[7], Judith Haasters[8], Kerstin Becker[1], Birgit Budde[1], Christian Becker[1], Holger Thiele[1], Shahid M. Baig[9,10], María Isidoro-García[11], Dominic Winter[6], Hans-Martin Pogoda[12], Sajjad Muhammad[13], Matthias Hammerschmidt[2,12], Florian Kraft[14], Ingo Kurth[14], Hilario Gomez Martin[15], Matias Wagner[8,16,17], Peter Nürnberg[1,2], Muhammad Sajid Hussain[1,2,*]

ARTICLE INFO

Article history:
Received 31 May 2023
Received in revised form
11 April 2024
Accepted 11 April 2024
Available online 16 April 2024

Keywords:
Autophagy
CYHR1
mRNA processing
Neurodevelopmental disorders
ZFTRAF1

ABSTRACT

Purpose: Neurodevelopmental disorders exhibit clinical and genetic heterogeneity, ergo manifest dysfunction in components of diverse cellular pathways; the precise pathomechanism for the majority remains elusive.

Methods: We studied 5 affected individuals from 3 unrelated families manifesting global developmental delay, postnatal microcephaly, and hypotonia. We used exome sequencing and prioritized variants that were subsequently characterized using immunofluorescence, immunoblotting, pulldown assays, and RNA sequencing.

Results: We identified biallelic variants in *ZFTRAF1*, encoding a protein of yet unknown function. Four affected individuals from 2 unrelated families segregated 2 homozygous frameshift variants in *ZFTRAF1*, whereas, in the third family, an intronic splice site variant was detected. We investigated ZFTRAF1 at the cellular level and signified it as a nucleocytoplasmic protein in different human cell lines. ZFTRAF1 was completely absent in the fibroblasts of 2 affected individuals. We also identified 110 interacting proteins enriched in mRNA processing and autophagy-related pathways. Based on profiling of autophagy markers, patient-derived fibroblasts show irregularities in the protein degradation process.

Conclusion: Thus, our findings suggest that biallelic variants of *ZFTRAF1* cause a severe neurodevelopmental disorder.

© 2024 Published by Elsevier Inc. on behalf of American College of Medical Genetics and Genomics. This is an open access article under the CC BY-NC-ND license (http://creativecommons.org/licenses/by-nc-nd/4.0/).

The Article Publishing Charge (APC) for this article was paid by University of Cologne and DFG Research Unit.

*Correspondence and requests for materials should be addressed to Muhammad Sajid Hussain, Cologne Center for Genomics (CCG), University of Cologne, Faculty of Medicine and University Hospital Cologne, Weyertal 115b, 50931 Cologne, Germany. *Email address:* mhussain@uni-koeln.de

Affiliations are at the end of the document.

doi: https://doi.org/10.1016/j.gim.2024.101143

1098-3600/© 2024 Published by Elsevier Inc. on behalf of American College of Medical Genetics and Genomics. This is an open access article under the CC BY-NC-ND license (http://creativecommons.org/licenses/by-nc-nd/4.0/).

Introduction

Neurodevelopmental disorders of genetic origin have been instrumental in revealing the complexities of human brain development. Neurodevelopmental disorders are clinically and genetically heterogeneous, caused by the disruption of early brain developmental events that can variably result in malformations of cortical development.[1]

ZFTRAF1 (MIM 616635) encodes zinc-finger tumor necrosis factor receptor-associated factor-type-containing protein 1, which is functionally poorly characterized, with scarce information available in the literature. This gene was previously known as *CYHR1* (cysteine and histidine-rich 1 protein) and *CHRP* (cysteine and histidine-rich protein). *ZFTRAF1* was initially identified from the human brain cDNA library, showing predominant expression in the brain.[2] The encoded protein was first discovered as a perinuclear and cytoplasmic component of the NIH3T3 cells and has shown up as a binding partner of galectin-3 in a yeast 2-hybrid screen aimed at identifying novel cytoplasmic proteins involved in intracellular trafficking.[3] It also makes a complex with galectin that binds to laminin under specific physiological conditions. The authors proposed that this complex may regulate the assembly or localization of the cytoplasmic precursors of proteasomes or spliceosomes.[4] Another independent study detected the immunoreactivity of EGFP-tagged ZFTRAF1 in nuclear speckles and found its colocalization with U1 small nuclear ribonucleoprotein particle. Furthermore, they revealed that importin subunit alpha-1 encoded by *Kpna2* is the binding partner of ZFTRAF1 and mediates its translocation to the nucleus with a plausible role in spermatogenesis. Based on the colocalization of green fluorescent protein (GFP)-ZFTRAF1/Chrp with U1 small nuclear ribonucleoprotein particle and its interaction with galectin-3, the authors implicated that ZFTRAF1 may have a crucial role in RNA processing during meiosis in the testis.[5] To date, *ZFTRAF1* variants have not been reported in the context of monogenic disorders except with pediatric low-grade gliomas.[6]

We report 5 affected individuals segregating pathogenic variants of *ZFTRAF1* manifesting severe neurodevelopmental disorder. We have also characterized ZFTRAF1 at the biochemical level and identified its presumable role in mRNA processing and protein degradation.

Material and Methods

Participants

We recruited 5 affected individuals from 3 unrelated families originating from Yemen (family 1), Germany (family 2), and Spain (family 3). The affected individual from Germany was recruited under the framework of the TRANSLATE-NAMSE project (http://tnamse.de/). Informed consent was obtained from the participants/guardians for research purposes. Bayley Scales of Infant and Toddler Development (BSID III) was used to evaluate intellectual disability status.

Genomic analyses

We performed exome sequencing of the affected member (IV-2) of family 1, the proband-parent trio for family 2, and the proband of family 3 as described previously.[7,8] We have provided the brief protocols in the Supplemental Method.

Homozygosity mapping

We performed genome-wide linkage analysis by genotyping 3 individuals (III-2, father, IV-2, P1, and IV-3, P2) from family 1 using HumanCoreExome 24 v.1.1 BeadArray (Illumina) following the manufacturer's instructions. We described the detailed procedure of data handling and statistical evaluation elsewhere.[9,10]

RNA extraction, cDNA synthesis, and reverse-transcription polymerase chain reaction (RT-PCR)

We used the PAXgene Blood RNA system (Qiagen) to extract the RNA from the blood of the affected individual from family 3 and the respective control. cDNA was synthesized using the previously published protocol.[11] To investigate splicing defects, we performed RT-PCR, using oligos identifying exons 1 and 4 of the *ZFTRAF1* (Supplemental Table 1). To quantify the wild-type transcript in P5 and mutant transcript in P4 and P5, we performed qPCR using primers targeting only exon 3 of the *ZFTRAF1* using the already described protocol.[11] Oligonucleotide sequences are enlisted in Supplemental Table 1.

Vector constructions and site-directed mutagenesis assay

We cloned an open reading frame of wild-type (NM_001330618.1) *ZFTRAF1* in pEGFP-C1. Using site-directed mutagenesis (Promega) protocol, we incorporated the frameshift variant, NM_001330618.1:c.1085_1086del, of *ZFTRAF1* in this plasmid. We provided the oligonucleotide sequences necessary for site-directed mutagenesis in Supplemental Table 1. Plasmids were propagated in prokaryotic cells (XL1-blue) and extracted from bacterial cells using a midiprep kit (Macherey-Nagel NucleoBond Xtra Midi, ThermoFisher Scientific, 740410.50).

Cell culture, immunofluorescence, immunoblotting, and microscopy

Human cell lines, HeLa, HaCaT, MCF-7, and U-373, along with primary fibroblasts of the affected individuals from family 2, family 3, and healthy individuals (controls), were

cultured using the standard methods described previously.[11] Notably, all of the biopsies were taken from the forearms of all the affected and unaffected healthy individuals (controls). To investigate the subcellular localization of ZFTRAF1 (endogenous and transiently expressed) and to analyze the abnormalities in patient-derived primary fibroblasts, we performed immunofluorescence (IF).[12] We described the protocol of IF in the Supplemental Method.

The procedure of immunoblotting is discussed previously in detail.[9] Method of immunoblotting, along with the information on antibodies and microscopy, are located in the Supplemental Method Section.

We performed a fractionation assay described previously to observe the relative expression of ZFTRAF1 in different subcellular compartments.[12] Resultant proteins from nuclear and cytoplasmic fractions were subjected to immunoblotting.

Pulldown assay and mass spectrometry

For pulldown assay, we transiently transfected HeLa cells with eukaryotic expression plasmids (pEGFP-C1) carrying open reading frames of both wild-type and mutant *ZFTRAF1* along with only pEGFP-C1, serving as a negative control, using 1 mg/mL polyethylenimine (PEI; 23966; Polysciences). After 24 hours of transfection, cells were lysed and incubated with the GFP-Trap Agarose beads (gta-20, Chromotek) using the recommended procedure of the Chromotek. Three independent technical replicates of each sample (wild type, mutant, and only GFP) were subjected to mass spectrometry (MS) analysis, following the procedure described previously.[12]

Proteome analysis

To analyze global trends of protein regulation, the proteome analyses of the affected individual (P5, family 3)-derived fibroblasts along with control were performed. The procedure of protein sample preparation is described in the Supplementary Methods section, whereas the process of MS analysis is described elsewhere.[13] The resulting peptides were analyzed by liquid chromatography-tandem mass spectrometry using an Ultimate 3000 RSLCnano ultra-high performance liquid chromatography system coupled to an Orbitrap Fusion Lumos (both Thermo Fisher Scientific) by data-independent acquisition and the resulting data by Spectronaut (version: 15.5.211111.50606, Biognosys), as described previously.[14] For spectral library generation, Swiss-Prot H. sapiens (20,960 entries, released 2020) were used in combination with a database containing common contaminants. The proteins were considered significantly regulated with absolute log2 ratios > 0.585 and Q values < 0.05.

Transcriptome analysis

RNA was extracted from primary fibroblasts derived from the affected individuals of families 2 and 3, as well as 4 different appropriate controls. A total of 1 µg RNA was subjected to bulk RNA sequencing. We sequenced 3 technical replicates of each sample and merged them into one, except for controls 3 and 4, in which only 1 sample was used for the analyses. We also merged both patient samples into 1 group to analyze the differentially expressed genes (DEGs). We have provided the detailed procedure previously.[15,16] A brief procedure is also mentioned in the Supplemental Method section.

To investigate the role of *ZFTRAF1* in splicing, we subjected the RNA of both affected members and the control for long-read nanopore sequencing using Oxford Nanopore Technologies (ONT). Libraries were prepared according to the manufacturer's protocol for PCR-cDNA sequencing (SQK-PCS109 ONT), starting with 50 ng total RNA and performing 18 PCR cycles. Final libraries were quantified and analyzed for size distribution (Tape Station, Agilent). Each library was loaded onto 1 flow cell (FLO-MIN106) with 100 fmol and run on a GridION device (ONT) using a Flow Cell Priming kit EXP-FLP002. Base calling was done with Guppy v6.4.6. The high-accuracy (HAC) model was selected for base calling. Differential splicing and isoform usage analysis were done by flair.[17] Briefly, raw data were basecalled using Guppy in the high-accuracy mode (HAC). Pychopper (v 2.7.7) (ONT) retained only full-length cDNA reads from the FASTQ files. The filtered data were further analyzed using flair. As only 1 replicate per sample was available, diff_iso_usage and diffsplice_fishers_exact of flair were used to find differently expressed isoforms and differently spliced transcripts. The data were visualized with flair plot_isoform_usage.

Results

Clinical manifestations of individuals harboring variants of *ZFTRAF1*

Family 1, a 4-generation family recruited from Yemen, has 3 affected members (P1;IV-2, P2;IV-3, and P3;IV-4) born to consanguineous parents (Figure 1A). All of the affected individuals manifested global developmental delay, variable degrees of intellectual disability, muscular hypotonia, and postnatal progressive microcephaly examined only at the time of 2 different latest medical examinations (Figure 1A, Table 1). These affected members did not show microcephaly at birth. Their motor skills were observed to be impaired; all 3 affected individuals cannot walk unaided. Impairment of walking is progressive and gets severe with time. Aggressive behavior was observed in the index-affected member. The affected individual of family 2 (P4) is a female born to nonconsanguineous parents and manifests global developmental delay and hyperreflexia (Table 1). She did not show any microcephaly (HC −1 SD) at birth, but a postnatal microcephaly of −2.4 SD was noted at the age of 4 years. Neuroimaging performed at the age of

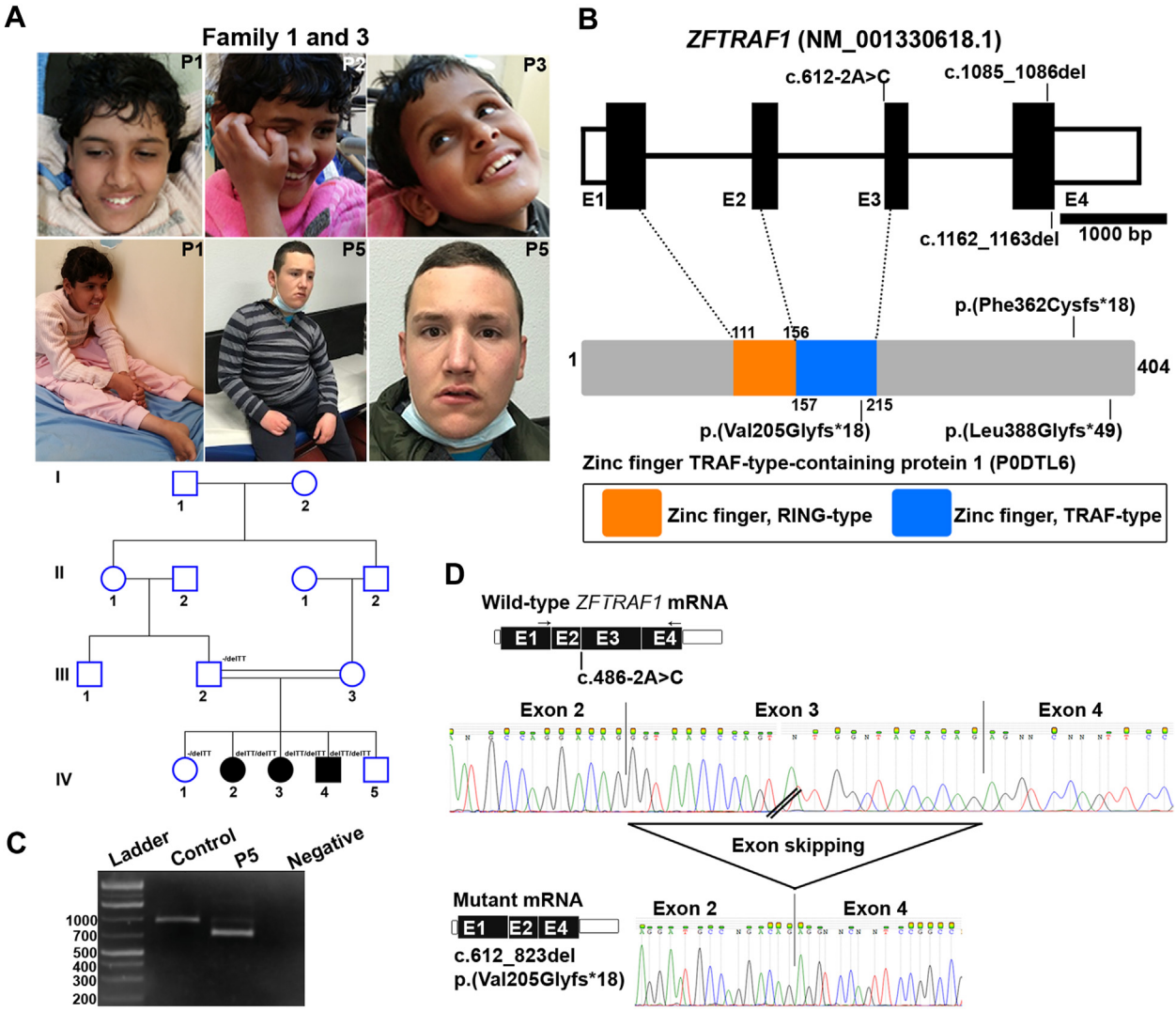

Figure 1 Clinical findings of family 1 and 2 along with the genomic data of *ZFTRAF1* variants. A. The upper panel shows the affected individuals of family 1 (individuals 1, 2, and 3) and family 3 (individual 5). The lower panel is a 4-generation simplified pedigree of family 1 recruited from Yemen. Genotypes of each tested individual are shown above the symbol. B. Schematic representation of human *ZFTRAF1* and the encoded protein predicted by the InterPro showing identified variants. InterPro predicted only 2 domains: zinc finger, RING-type, and zinc finger, tumor necrosis factor receptor-associated factor (TRAF)-type. The scale bar for the exon is given, whereas the introns are drawn without any scale. C. Agarose gel (2%) shows the reverse-transcription polymerase chain reaction (RT PCR) products belong to both control and affected individual 5. 1 kb plus DNA Ladder (Invitrogen, 10787018) is used. D. Sanger traces of RT-PCR product of wild-type *ZFTRAF1* showing junctions between exons 2, 3, and 4. Below the wild type, traces for the aberrant transcript generated in affected individual 5 are shown where exon 3 is skipped. Hypothetical genomic representations of wild-type and mutant *ZFTRAF1* are also shown. Arrows indicate the position of oligos used for RT-PCR.

13 months did not show any gross brain abnormality. The affected individual of family 3 (P5) is an 18-year-old male from Spain manifesting encephalopathy (Figure 1A), epilepsy (generalized seizures from 2014 to 2016), severe intellectual disability, global hypotonia (strength and reflexes are normal), and no signs of microcephaly (Table 1). Neuroimaging performed at the age of 8 years revealed no gross abnormality. His intellectual disability made it difficult to conduct a reliable neurological exploration. The affected member showed motor skills deterioration and needed help standing from the seat, although there were no clear Gowers' signs, and he walked with aid.

Identification of protein-truncating variants of *ZFTRAF1*

Exome sequencing of family 1 revealed a homozygous frameshift variant of *ZFTRAF1* (Ref seq transcript for all variants is NM_001330618.1) c.1085_1086del p.(Phe 362Cysfs*18) (Figure 1B, Table 1), which cosegregated with the disease in the family (Supplemental Figure 1A). Through GeneMatcher,[18] we recruited 1 German (P4, family 2) and 1 Spanish affected individual (P5, family 3). A homozygous frameshift variant c.1162_1163del p.(Leu388Glyfs*49) (Figure 1B) was identified in the affected index individual from

Table 1 Clinical and genetic profile of *ZFTRAF1* mutated individuals

Family ID	Family 1			Family 2	Family 3
Ethnicity	Yemeni			German	Spanish
Feature	Patient 1 (IV-2)	Patient 2 (IV-3)	Patient 3 (IV-4)	Patient 4 (P4)	Patient 5 (P5)
ZFTRAF1 (NC_000008.11 and NM_001330618.1) variant	g.144450508_144450509del c.1085_1086del p.(Phe362Cysfs*18)			g:144450431_144450432del c.1162_1163del p.(Leu388Glyfs*49)	g.144452572A>C c.612-2A>C p.(Val205Glyfs*18)[a]
Age at examination (years)	15	14	12	4	18
Gender	Female	Female	Male	Female	Male
Microcephaly	Microcephaly (−3 SD)	Microcephaly (−3.5 SD)	Microcephaly (−4 SD)	Microcephaly (−2.4 SD)	-
Behavior	Abnormal	NA	NA	Normal	NA
Developmental delay	+	+	+	+	+
Intellectual disability	Severe	Severe	Severe	Mild	Mild
Muscular hypotonia	+	+	+	+	+
Motor deterioration	+	+	+	No	+

"+" means the manifestation of a particular condition or disease and "–" shows the absence of phenotype.
NA, information not available.
[a]This variant has resulted because of the formation of an aberrant transcript.

family 2 (Table 1). The variant was inherited from the unaffected father and was present in homozygosity because of a paternal isodisomic uniparental disomy of chromosome 8 (UPD8), as confirmed by trio exome analysis. The affected individual from family 3 harbored a homozygous splice variant c.612-2A>C p.? (Figure 1B, Table 1). All of these variants of *ZFRTAF1* are absent in the Genome Aggregation Database (gnomAD), Iranome, dbSNP156, the Greater Middle Eastern Variome, and in our in-house database (>5K exomes) of the Cologne Center for Genomics.

In parallel to exome sequencing, we performed genome-wide linkage analysis by genotyping the available members (2 affected individuals and father) of family 1. Data analysis revealed 4 homozygous segments at chromosomes 8, 11, 18, and 20, each with a maximum possible logarithm of the odds score of 1.8 (Supplemental Figure 1B). The homozygous segment of chromosome 8 is defined by single-nucleotide variation (formerly SNP) markers, rs6988219 (138,229,583 bp) and qter, chromosome 11 by rs1055574 (17,494,286 bp) and rs11026758 (22,732,034 bp), chromosome 18 by rs2109616 (9,807,170 bp) and rs1017414 (26,825,636 bp), and chromosome 20 is bounded by rs805761 (5,697,112 bp) and rs235772 (6,782,072 bp). Note that the physical positions of the single-nucleotide variation markers are taken from the National Center for Biotechnology Information human genome build GRCh38. The *ZFTRAF1* (NM_001330618.1) resides within the homozygous segment of 8.04 Mb (GRCh38) detected on chromosome 8 (Supplemental Figure 1C), thus further supporting the candidacy of this gene.

The 2-base-pair deletion, NM_001330618.1: c.1085_1086del, identified in family 1, is located in the last exon of *ZFTRAF1*, exon 4 (Figure 1B) and presumably causes a frameshift running into a premature termination codon NP_001317547.1:p.(Phe362Cysfs*18). Because the variant is situated in the last exon, the mutant transcript will likely escape nonsense-mediated decay. Still, the resultant protein would lack the C-terminal part (approximately 43 amino acids). Whereas the variant, NM_001330618.1:c.1162_1163del p.(Leu388Glyfs*49), identified in the affected individual (P4) also present in exon 4 (Figure 1B), causes frameshift, predictably resulting in the extension of protein from 404 amino acids to 435 aa. The additional residues in mutant protein may result in irregular structure, improper folding, and/or enhanced proteolytic degradation. The intronic variant, NM_001330618.1:c.612-2A>C, of P5, located within the canonical splice acceptor site, was predicted to be altering the canonical splice acceptor site by NetGene2-2.42 server (Supplemental Figure 1D). We performed RT-PCR with cDNA extracted from the affected individual's blood and control to investigate this. Similar to the control, we observed a product of the expected size (1000 bp) in the affected individual, but the signal intensity of the band is faint (Figure 1C). Additionally, we observed a band of stronger intensity of 788 bp only in the affected individual (Figure 1C). Sanger sequencing of the small PCR product (788 bp) revealed skipping of exon 3

(NM_001330618.1:c.612_823del) of *ZFTRAF1* in the affected individual resulting in a frameshift and introducing a premature stop codon NP_001317547.1:p.(Val205Glyfs*18) (Figure 1D). We assume this aberrant transcript may escape nonsense-mediated decay and result in the synthesis of truncating protein, which might be unstable. Consequently, the protein translated by the wild-type transcript may not be enough to perform the normal function of the ZFTRAF1. We performed quantitative PCR to measure the amount of *ZFTRAF1* transcript. Data revealed no significant differences in the amount of *ZFTRAF1* in both affected members P4 and P5 compared with the control (Supplemental Figure 1E). Furthermore, we also quantified the wild-type *ZFTRAF1* transcript in P5 using primers that only targeted exon 3. Data revealed significantly reduced expression of *ZFTRAF1* in P5 compared with control (Supplemental Figure 1F).

Transient expression of GFP-ZFTRAF1

To functionally characterize ZFTRAF1 and its variant (NP_001317547.1:p.(Phe362Cysfs*18)), we first investigated the subcellular localization of the wild-type protein. The transient expression GFP-ZFTRAF1 in HeLa cells showed that the wild-type GFP-ZFTRAF1 is expressed in the nucleus and cytoplasm (dot-like structures) (Figure 2A). Additionally, wild-type GFP-ZFTRAF1 was also observed only in the nuclei of a few cells (data not shown). However, the mutant protein was seemingly absent in the nucleus, and a few puncta were observed only in the cytoplasm (Figure 2A). Mutant GFP-ZFTRAF1 was not only mislocalized but also reduced in size and quantity (Figure 2A and B). We could assume the mutant protein is unstable and might be subject to proteolytic degradation. Therefore, a small amount remains visible in the cytoplasm.

ZFTRAF1 localization in different mammalian cell lines and patient-derived fibroblasts

The subcellular distribution of endogenous ZFTRAF1, as determined in HaCaT, MCF-7, and U-373 cells, displayed immunoreactivity as dot-like structures inside nuclei and cytoplasm (Figure 2C). Furthermore, the colocalization of several puncta of endogenous ZFTRAF1 with a nuclear speckles marker, SF3B4 (splicing factor 3B subunit 4), was observed (Supplemental Figure 2A). The immunoblotting was performed for HeLa and MCF-7, which also showed the presence of ZFTRAF1 in both nuclear and cytosolic fractions (Figure 2D). Furthermore, similar to HaCaT and MCF-7, ZFTRAF1 puncta were also observed in the nuclei and cytosol of the control human primary fibroblasts (Figure 2E). However, ZFTRAF1 puncta were absent in primary fibroblasts derived from affected individual P4. As expected, primary fibroblasts derived from affected individuals P5 showed no immunoreactivity of ZFTRAF1 (Figure 2E). The same was corroborated by immunoblotting of protein lysates of primary fibroblasts derived from both affected individuals (Figure 2F). Only a faint band, corresponding to wild-type ZFTRAF1, was visible in the protein lysate of affected individual P5 segregating the splice variant depicting the residual amount of protein from the wild-type transcript shown by the RT-PCR (Figure 2F). Compared with control, quantification of mutant ZFTRAF1 immunoreactivity revealed 0.96-fold and 0.73-fold decreased expression in P4 and P5, respectively (Supplemental Figure 2B).

Analysis of ZFTRAF1 interactome

To reveal the cellular role of ZFTRAF1 and identify interacting partners, wild-type GFP-ZFTRAF1, mutant (NP_001317547.1:p.(Phe362Cysfs*18)), and only GFP proteins were subjected to pull down coupled with MS (Supplemental Figure 3A). Wild-type, mutant GFP-ZFTRAF1, and negative control (GFP only) data sets were validated by principle component analysis (PCA) (Supplemental Figure 3B). MS analyses showed 1100 unique proteins (Supplemental Figure 3C and D). Using stringent filtering criteria and removing binding partners of GFP only, 110 interaction partners of wild-type ZFTRAF1 were identified, out of which 60 were losing binding affinity with GFP-tagged mutant protein (Supplemental Figure 3D, Supplemental Table 2). In these 110 proteins, we also found 5 proteins (APEH, CLINT1, H1FX, SHMT2, and VPS35) predicted as binding partners of ZFTRAF1 by an online available database, GPS-Prot (http://gpsprot.org/).

Functional enrichment of proteins showing binding affinities with wild-type ZFTRAF1 mainly revealed 2 interesting pathways: (1) ubiquitination and proteasome degradation and (2) mRNA processing (Supplemental Figure 3E). Cellular components enrichment showed that these binding proteins are nuclear, cytoplasmic, lysosomal/exosomal, and components of the spliceosome (Supplemental Figure 3F).

Lysosomal accumulation in patient-derived primary fibroblasts

Based on the enrichment results of interacting partners, primarily, lysosome, an organelle performing a critical role in the clearance of cellular debris, was investigated; lysosomal markers lysosome-associated membrane glycoprotein 1 (LAMP1) and lysosome-associated membrane glycoprotein 2 (LAMP2) were examined in the primary fibroblasts derived from P4 and P5. Interestingly, the immunofluorescence showed a higher expression of both proteins in patients' fibroblasts compared with the control (Figure 3A, upper and middle panels, Supplemental Figure 4A). These data were further corroborated by immunoblotting, in which a stronger immunoreactivity was noted for LAMP2 in the protein lysates of both affected individuals compared with the control (Figure 3B). Quantification of LAMP2 immunoreactivity revealed 7.07-fold and 7.91-fold increased expression in P4 and P5, respectively, compared with control (Supplemental Figure 2B).

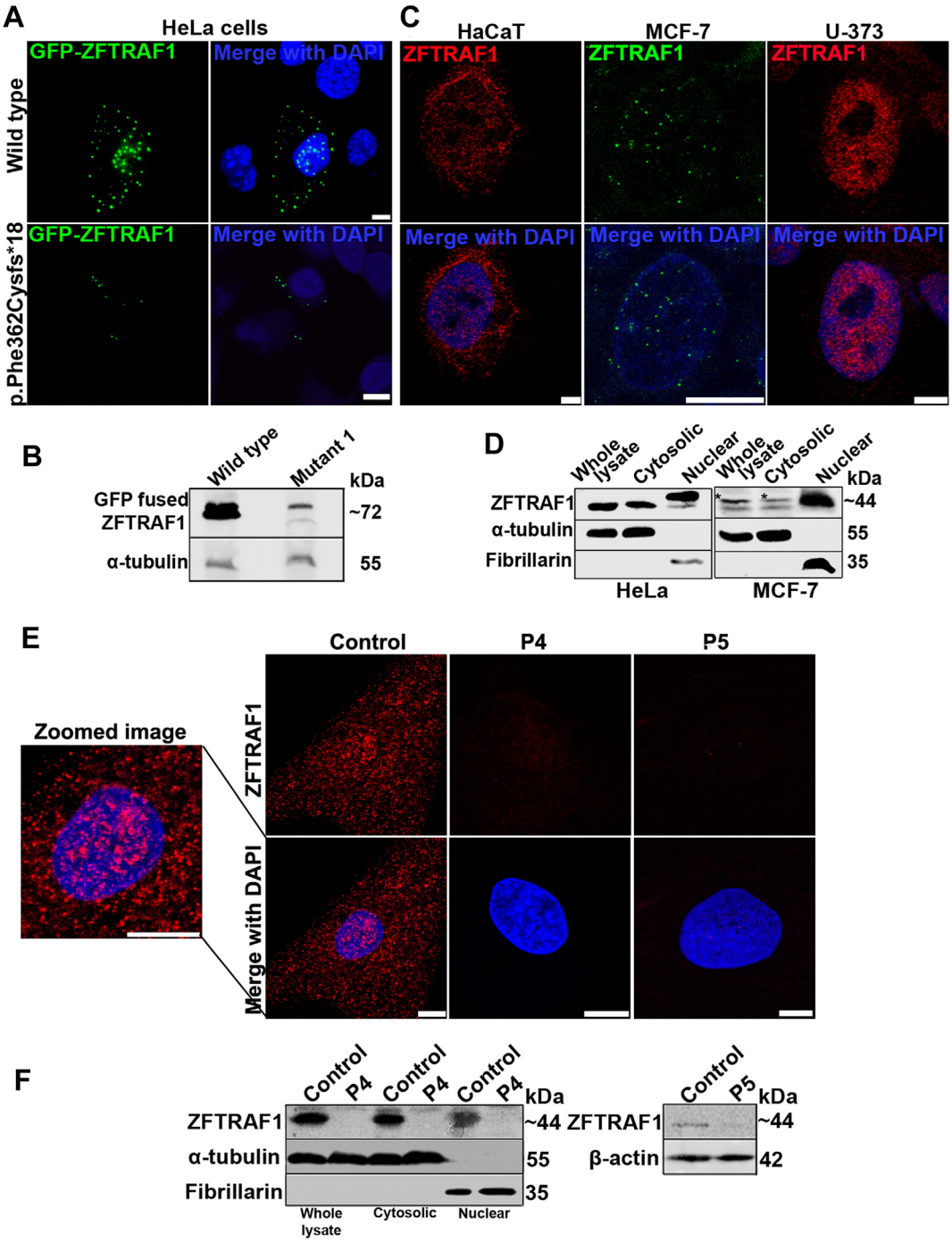

Figure 2 **Subcellular localization of ZFTRAF1.** A. Confocal images of HeLa cells showing transient expression of wild-type and mutant GFP-ZFTRAF1. The scale bar is 10 μm. B. Immunoblots showing wild-type and mutant GFP-ZFTRAF1. Note that the mutant protein (column 2) is reduced in size and amount compared with the wild type (column 1). The experiment is performed 3 times. Asterisks show the mutant GFP-ZFTRAF1 in column 2. α-Tubulin acts as a marker of equal protein loading. C. Confocal microscopy images of HaCaT, MCF-7, and U-373 cells show the localization of endogenous ZFTRAF1. The scale bar is 10 μm. D. Fractionation assay validates the expression of ZFTRAF1 both in the nuclei and cytoplasm of the HeLa and MCF-7 cells. α-Tubulin is used as a marker of equal protein loading, and fibrillarin is the nuclear marker. Asterisks represent the bands of ZFTRAF1 detected in the whole-cell and cytosolic lysates. The experiment is performed only once. E. Confocal images showing the endogenous expression of ZFTRAF1 in control and patients-derived primary fibroblasts. On the left side, a zoomed image of the control primary fibroblast cell shows a clear nuclear and cytoplasmic localization of ZFTRAF1. The scale bar is 10 μm. Only the representative images are shown. Notably, the ZFTRAF1 antibody can detect the mutant protein only in P4. F. Immunoblotting showing the ZFTRAF1 in nuclear and cytoplasmic fractions. Notably, ZFTRAF1 is absent in P4 (left panel) and reduced in P5 (right panel). Two different blots are shown. Equal protein loading is confirmed using α-tubulin and β-actin, whereas fibrillarin is used as a nuclear marker. Notably, the immunogen of the tested antibody is located at the C terminus of ZFTRAF1; therefore, it may not be able to show the immunoreactivity with the truncated version of the ZFTRAF1 protein being synthesized in P5.

Investigation of autophagy regulators in patient's fibroblasts

Because we observed drastic levels of lysosomal accumulation in the patient's fibroblasts, we further investigated autophagy-related markers to validate the accumulation of cellular debris. In this regard, we analyzed SQSTM1\p62, which showed markedly stronger p62 puncta in both patient-derived fibroblasts compared with the control (Figure 3A, lower panel). Second, galectin-3, which is also a well-known sensor protein for lysophagy, was also upregulated in the primary fibroblasts of P4 as analyzed by immunoblotting (Figure 3C). Quantification of immunoblots revealed 3.29-fold increased expression of galectin-3 in P4 compared with control (Supplemental Figure 2B). Furthermore, the immunoreactivity of ATG16L showed reduced (0.91-fold decrease) expression and increased expression of LC3β in P4 compared with the control, suggesting impaired autophagy function (Figure 3D and E, Supplemental Figure 2B). Quantification of LC3β, also known as LC3-II, immunoreactivity revealed 2.53-fold increased expression in P4 compared with control (Supplemental Figure 2B).

We performed electron microscopy to reveal the cellular abnormalities in fibroblasts derived from affected individual P4. Data showed an accumulation of dark round bodies, which is indicative of lysosomal aggregation, and reduced nuclear size (Figure 3F). IF analysis revealed that nuclear size was considerably reduced in both patients' fibroblasts compared with the control (Supplemental Figure 4B, left panel). This was further validated by taking the statistical data of the nuclear size of the control and both patients' fibroblasts. As expected, it was significantly reduced in the affected individuals compared with the control (Supplemental Figure 4B, right panel).

Proteome profiling of primary fibroblasts

For proteome profiling, individual data sets (4 technical replicates each of control and patient-derived primary fibroblasts) were normalized (Supplemental Figure 5A) to compensate for differences in sample loading and common protein groups subjected to further analyses (Supplemental Figure 5B). The heatmap was generated to observe the dysregulated expression (Supplemental Figure 5C). Proteome analyses showed a total of 4587 proteins (unfiltered ratios) obtained as unique data points (Figure 4A). The proteins were filtered for an absolute log2 ratio of > 0.585 (fold change $= 1.5$) and a Q value of < 0.05, revealing 413 significantly downregulated and 61 upregulated proteins (Figure 4B, Supplemental Table 3).

Among the highly downregulated proteins were lipocalin-1 (LCN1), nuclear RNA export factor 1 (LYZ), small proline-rich proteins (SPR2E; SPR2B; SPR2A), and brain 3 protein (BRI3) (Figure 4C). The most highly upregulated protein was death-associated protein 1 (DAP1) (Figure 4C). Furthermore, we observed other highly upregulated proteins too, namely, KRT33A, BCS1L, and MTMRD (Figure 4C). We noted significantly dysregulated expression of 8 binding partners of ZFTRAF1 (Figure 4D, Supplemental Table 4). However, the functional relevance of these proteins and ZFTRAF1-mutated affected individuals needs further validation.

The MS-identified binding partners of ZFTRAF1, including VCIP1, NDUF2, NDUF4, NDUAC, NDUV1, HERC4, I2BPL, UBP10, UBP24, UBP48, RL40, and UB2E1, also showed discernible dysregulated expression (Figure 4E).

Furthermore, we performed the functional enrichment of dysregulated proteins using the ShinyGo enrichment tool (http://bioinformatics.sdstate.edu/go/), which, expectedly, showed pathways related to RNA/mRNA export, macroautophagy, and processes utilizing the autophagic mechanism (Figure 4F). Additionally, this showed enrichment of intracellular transport and establishment of proteins to vacuoles, which indicates that ZFTRAF1 may act as a nucleocytoplasmic protein participating in autophagic events.

Because we observed an accumulation of lysosomes in patient-derived fibroblasts, the expression trends of lysosome-related proteins were also analyzed, presenting considerable dysregulation of 12 lysosomal proteins upregulated, whereas 19 proteins were significantly downregulated (Supplemental Table 5). The disease relevance of most of these proteins has already been reported, indicating the damaging effects of dysregulation of these proteins globally (Supplemental Table 5).

Based on protein classes (transferases, synthases, dehydrogenases, kinases, and RNA binding proteins), 68 proteins were prominent in the proteome data presenting visible changes in the expression (Supplemental Table 6).

Transcriptome profiling

Transcriptome profiling of RNA obtained from both patients' derived fibroblasts (3 technical replicates each of P4 and P5) was performed along with 4 biological replicates of control to identify the globally dysregulated expression of genes. All the replicates were validated by PCA plot (Supplemental Figure 6A), and heatmaps for both affected individuals were generated, showing clear differential expression (Supplemental Figure 6B). These data showed 35,094 transcripts in P4 and P5 (Supplemental Table 7). Upon filtering (adjusted P value $\leq .05$ and fold change [FC] ≥ 1.5), we observed 116 downregulated and 21 upregulated RefSeq DEGs (Figure 5A and B, Supplemental Table 8). Pathway enrichment of these DEGs revealed involvement in transcription regulation and autophagic mechanism (Figure 5C).

GATA1 is the most highly upregulated (25-fold change [FC]) gene, which is a master regulator of genes involved in autophagy.[19] We analyzed downregulated genes and found *HOXC11* (FC: −8.3) to be the most differentially expressed gene (Figure 5A, Supplemental Table 7). The second and third highly downregulated genes were *HOTAIR* (−7.3 FC)

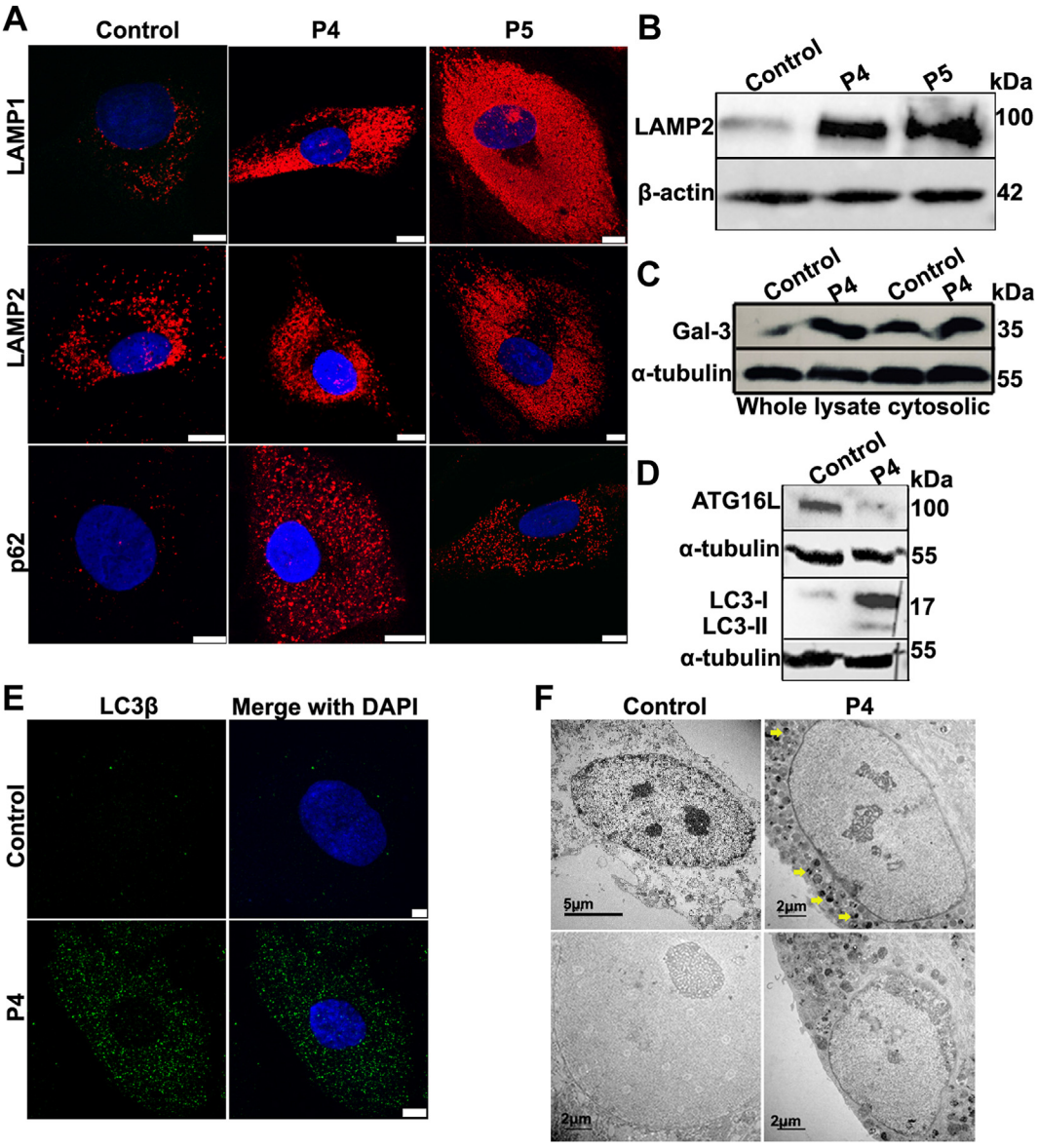

Figure 3 Autophagy defects in ZFTRAF1-mutated affected individuals. A. Confocal images show increased lysosome-associated membrane glycoprotein 1 (LAMP1), lysosome-associated membrane glycoprotein 2 (LAMP2), and p62 in primary fibroblasts derived from affected individuals (P4 and P5) compared with control fibroblasts. The representative images are shown only. The scale bar is 10 μm. B. Immunoblot shows increased LAMP2 in P4 and P5 compared with the wild type. Note that β-actin is used as a loading control. C. Immunoblot shows an increased amount of Gal-3 tested only in P4 compared with the control. Data from 2 independent experiments are shown on 1 blot. Note that α-tubulin is acting as a loading control. D. Immunoblots obtained from 2 different gels show reduced ATG16L in P4 compared with the wild type and an increased amount of LC3β, both cytosolic (LC3-I) and lipidated (LC3-II), in P4 compared with the control. Note that α-tubulin is used as a loading control. E. Confocal images showing increased puncta of LC3β tested only in P4 compared with the control. The scale bar is 10 μm. F. Upper panel, electron micrographs showing accumulation of cellular material close to the nuclear periphery indicated by yellow arrows in P4-derived primary fibroblasts. Lower panel, electron micrographs show reduced nuclear size in the affected individual compared with the respective control. The scale bar is indicated.

and *TRPM3,* well-established factors for activating autophagy.[6,20] Interestingly, *VANGL2*, another downregulated (−6.9) gene, is also reported to regulate the fate of LAMP2.[21] Most importantly, we found significant upregulation (Figure 5C) of autophagy-related genes (*SQSTM1*, *LAMP1, LAMP2, LC3B*, and *LGALS3*), validating our finding at the protein level in primary fibroblasts derived from affected members.

We found only 2 common genes (*OAS3* and *A2M*) in the transcriptome and proteome data. Furthermore, analyzing mutant *ZFTRAF1* transcript revealed a −0.000133446 fold (adj. *P* value 1) and −9.38783E−05-fold (adj. *P* value .999964) decrease in P4 and P5, respectively, statistically considered nonsignificant.

To uncover the novel role of *ZFTRAF1* in differential splicing, we performed long-read nanopore sequencing

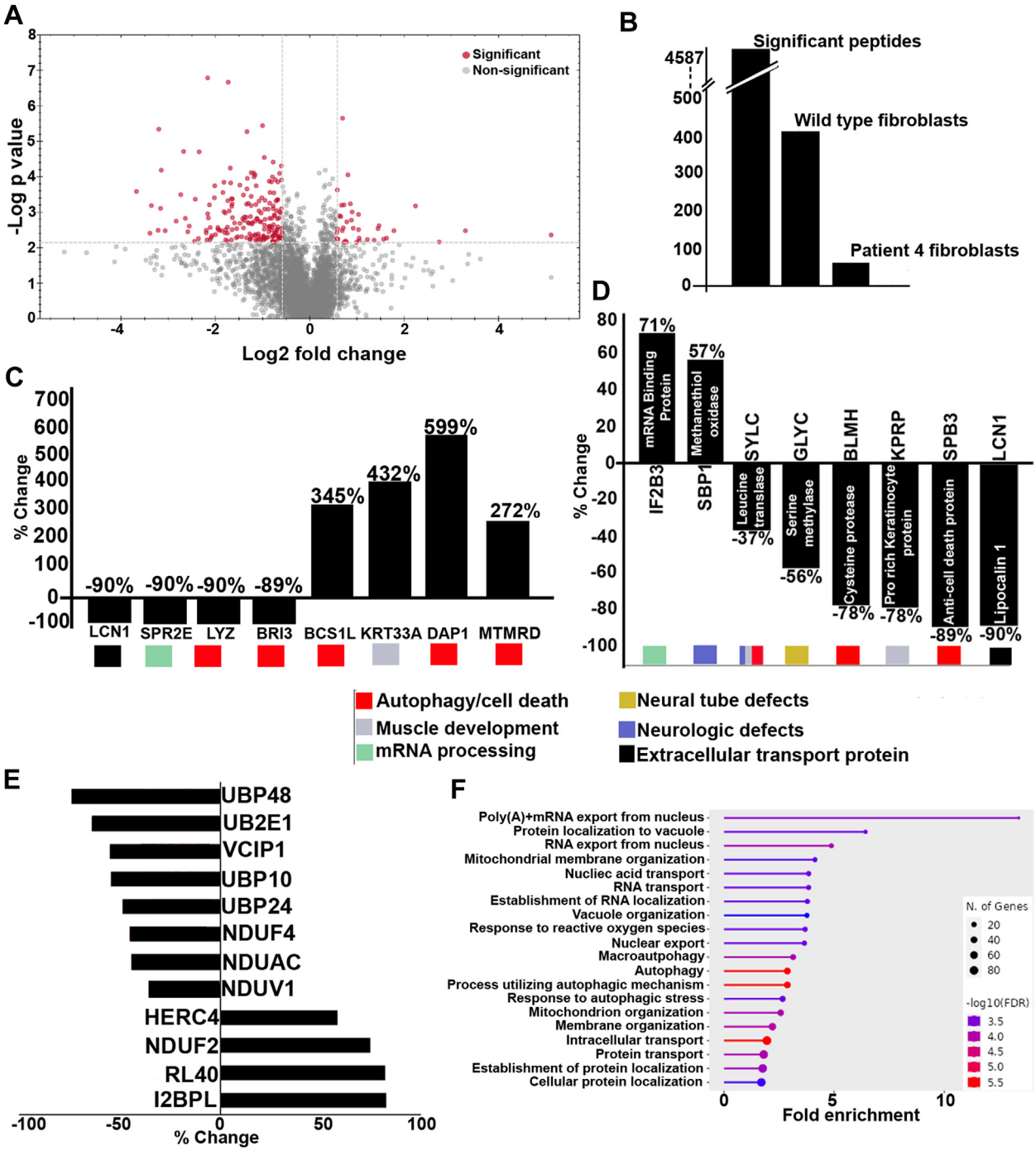

Figure 4 **Proteome data of P5-derived fibroblasts.** A. Volcano plot showing all identified proteins in which red dots show significantly differentially expressed proteins in contrast with gray dots. *P* values ≤ .05 and fold change ≥1.5. B. The bar graph shows all identified proteins (4587), 413 downregulated, and 61 upregulated. The proteins were filtered for an absolute log2 ratio of > 0.585 (≥1.5-fold change) and a *P* value of ≤ .05. C. The bar graph shows 4 highly upregulated and 4 highly downregulated proteins. Note that the *P* value is ≤ .05. D. Bar graph presenting trends of 8 mass-spectrometry-identified proteins in proteome data. Note that the *P* value is ≤ .05. E. Bar graph showing dysregulated ubiquitination-related proteins. Note that the *P* value is < .05. F. Functional enrichment of differentially expressed proteins.

using ONT. Data of both affected members revealed 4 types of alternative splice events: alternative 3′ splice site, alternative 5′ splice site, exon skipping, and intron retention (Figure 6A and Supplemental Tables 9 and 10). Approximately 1188 differentially spliced annotated genes in P4 (Supplemental Table 9) and 1618 genes in P5 (Supplemental Table 10) were detected. Interestingly, 643 genes were common in both affected members (Supplemental Table 11) enriched for spliceosome, ribosome, and pathways of neurodegeneration (Figure 6B).

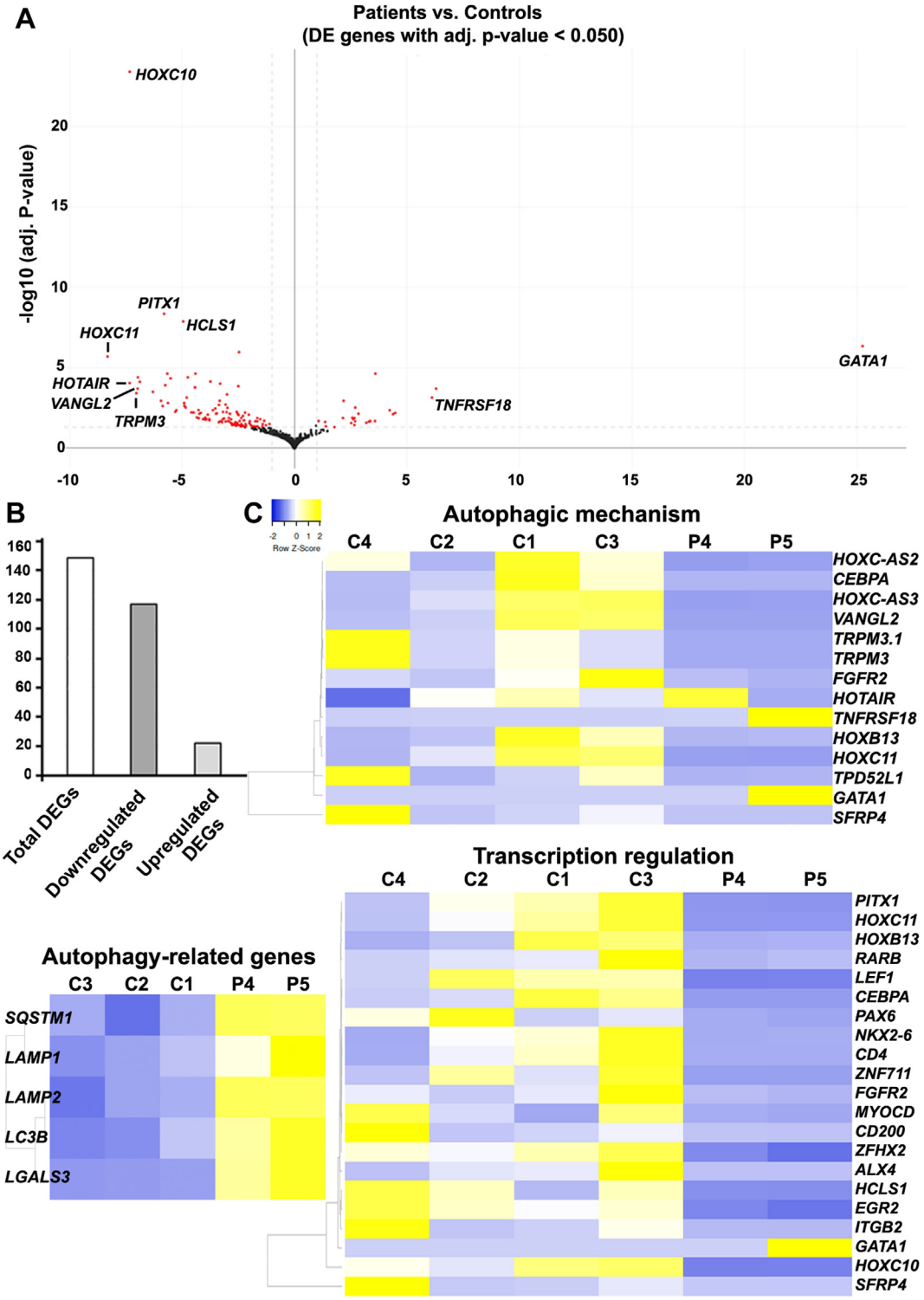

Figure 5 **Transcriptome profiling of P4 and P5.** A. Volcano plots present all the identified transcripts, in which red dots show significantly differentially expressed transcripts in contrast with the black dots representing nonsignificantly differentially expressed transcripts. Adjusted P value $\leq .05$ and fold change ≥ 1.5. B. The bar graph shows several upregulated and downregulated transcripts. Adjusted $P \leq .05$ and fold change ≥ 1.5. C. Heatmaps show DEGs related to autophagy and transcription regulation. Autophagy-related genes, shown in the lower left, were also significantly upregulated in the patient-derived primary fibroblasts tested at protein levels. Note that the color coding on the upper left shows up and downregulation of the targeted genes. $P \leq .05$ and fold change ≥ 1.5.

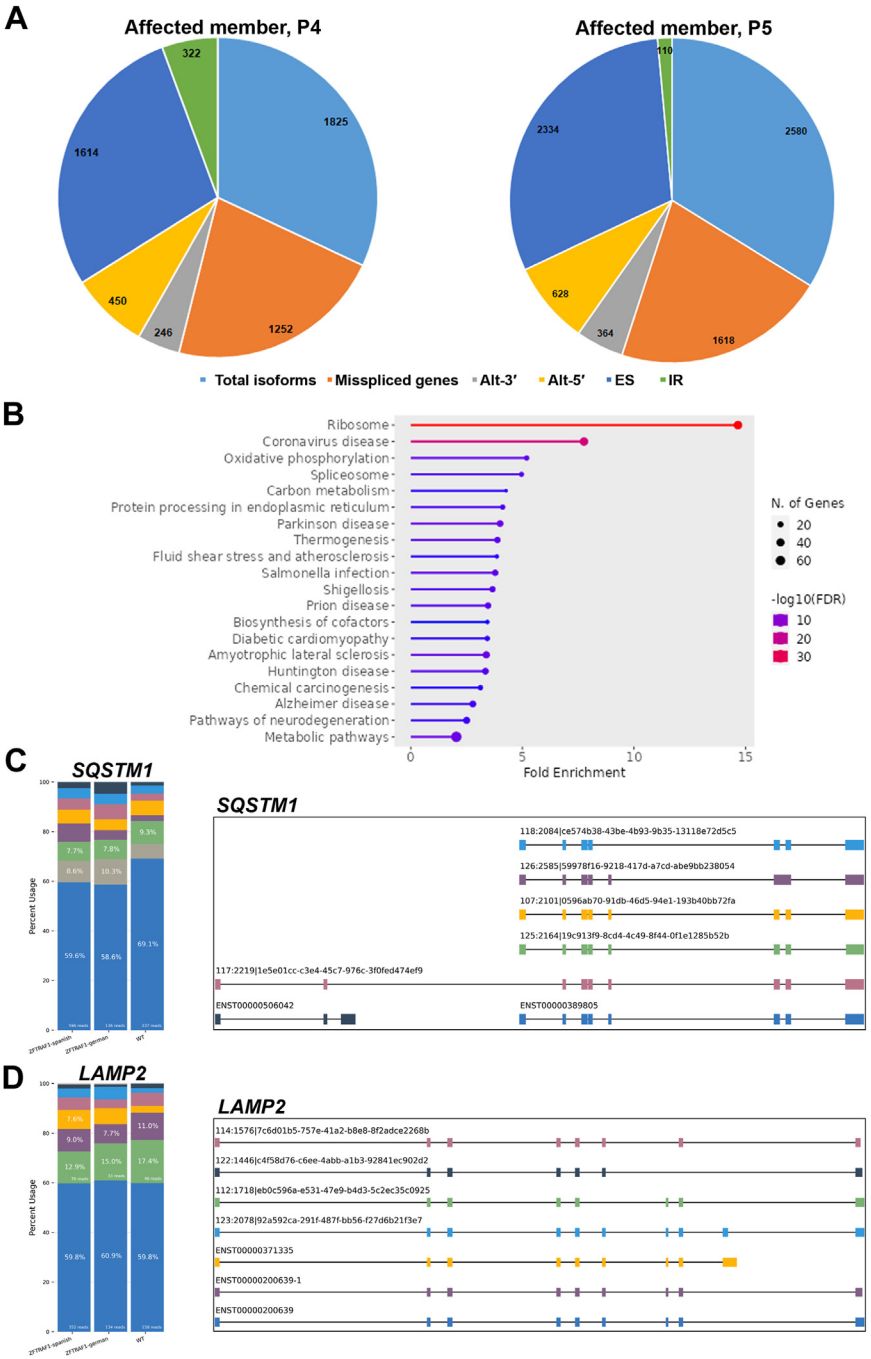

Figure 6 ONT data showing differential splicing in P4 and P5. A. Pie chart showing the alternative splice events in affected members, P4 (left side) and P5 (right side). Alt-3′, alternative 3′ splice site; Alt-5′, alternative 5′ splice site; ES, exon skipping; IR, intron retention. B. Enrichment (ShinyGO 0.77) of common differentially spliced genes found in P4 and P5. C. Isoform usage data of *SQSTM1* encoding p62 protein (left panel). Schematics of *SQSTM1* and differentially spliced transcripts (right panel) were detected in affected members P4 (*ZFTRAF1*-German), P5 (*ZFTRAF1*-Spanish), and control. D. The proportion of lysosome-associated membrane glycoprotein 2 (*LAMP2*) transcripts isoforms (left panel) and schematics of differentially spliced transcripts of *LAMP2* (right panel) detected in affected members P4 (*ZFTRAF1*-German), P5 (*ZFTRAF1*-Spanish), and control.

Furthermore, we focused on a few genes involved in autophagy (*SQSTM1*, *LAMP2*, *ATG12*, *DRAM2*, *LGALS1*, *MBOAT7*, *LGALS1*, and *GLMP*), translation machinery (*EIF1* and *EIF6*), and ubiquitination (*SUMO2* and *UBR4*). We investigated the aberrant transcripts produced in these genes. Seven aberrant transcripts of *SQSTM1,* encoding p62 protein, were detected (Figure 6C). Similarly, investigating *LAMP2* revealed 4 aberrant transcripts (Figure 6D). Similarly, we found several aberrant transcripts of genes mentioned above with established roles in autophagy, translation machinery, and ubiquitination (Supplemental Figure 8).

Induced pluripotent stem cells generation from patient fibroblasts

The reprogramming of fibroblasts into induced pluripotent stem cells requires vigorous autophagy, mainly during the early phases of cell reprogramming.[22] Both patients' fibroblasts were induced using an RNA-based reprogramming vector. In the case of the control fibroblast, 10 to 20 clear, round, and tightly packed induced pluripotent stem cells (iPSCs) colonies were observed (Supplemental Figure 7). In comparison with the control, both patients' fibroblasts could barely achieve pre-iPSCs, a phase in which the fibroblasts started to reshape into a smaller size (Supplemental Figure 7). However, these cells could not proceed beyond the pre-iPSCs phase, presumably because of defective autophagy in *ZFTRAF1*-mutated fibroblasts.

Discussion

We report 3 biallelic variants of *ZFTRAF1* in 5 affected individuals from 3 different families. All the affected members show developmental delay, variable degrees of intellectual disability, and muscular hypotonia. Phenotypic variability in terms of microcephaly and motor skills deterioration is observed. Interestingly, 1 affected member recruited from Spain did not show microcephaly. The remaining affected members manifest postnatal microcephaly. Unfortunately, we do not have any accurate data that depicts the age of onset of microcephaly. Deterioration of motor function was only observed in terms of standing and walking. Four of the 5 affected members are unable to walk or stand. We propose loss-of-function of *ZFTRAF1* as the likely underlying pathomechanism because the identified variants cause an early truncation and therefore could result in the synthesis of unstable protein. This hypothesis was further corroborated by the absence of ZFTRAF1 in primary fibroblasts derived from 2 affected individuals. However, we could not explore this possibility in the affected individual (P1) because of the unavailability of affected individual material from Yemen.

Previously, ZFTRAF1 has been reported to localize in the cytoplasm and perinuclear space in murine fibroblasts.[3] Here, we report its localization in both nucleus and cytoplasm in different mammalian cell lines, ie, HeLa, MCF-7, and human primary fibroblasts; however, the perinuclear staining suggested by the previous study was observed only in a few HeLa cells (data not shown). Contrary to the previous study showing the localization of GFP-ZFTRAF1 exclusively within the nuclei, we observed its localization within nuclei and in the cytoplasm.[5] We suggest that ZFTRAF1 is a nucleocytoplasmic protein performing dual nuclear and cytoplasmic functions.

We identified 110 potential binding partners of ZFTRAF1, showing enrichment for (1) mRNA processing (the nuclear function) and (2) ubiquitination and proteasomal degradation (cytoplasmic function). Interestingly, the former is supported by previous reports of its colocalization with U1 small nuclear ribonucleoprotein particle.[5] Out of 110 binding partners, 60 proteins showed decreased binding affinity with the mutant ZFTRAF1 in vitro. Nonetheless, because ZFTRAF1 is depleted in patient-derived fibroblasts, it suggests that the in vitro pathogenesis is not based on impaired binding.

Cellular debris/misfolded proteins are usually degraded by 3 different mechanisms, ie, the ubiquitin-proteasome system (UPS), macroautophagy, or chaperone-mediated autophagy.[23] Nonetheless, lysosomes mainly ensure the hygiene of cells,[24] which are degraded by lysophagy when worn out.[25] Our data showed an accumulation of lysosomes in the patients' derived fibroblasts, indicating inefficient lysophagy. Previous studies have reported that recruitment of p62 corresponds to early detectable ubiquitination on damaged lysosomes (DL),[26] which also appeared upregulated in the patient's fibroblasts, further validating the accumulation of DL.

The degradation of DL is conducted in 3 steps: (1) sensing (sensor proteins, such as galectins), (2) tagging (ubiquitination tag on damaged organelle), and (3) phagophore formation (recruitment of the autophagy machinery).[27] Interestingly, galectin-3, a sensitive reporter for lysosomal damage,[28] and a known binding partner of ZFTRAF1, was upregulated in the patient's fibroblasts, presumably because of increased accumulation of DL in affected individual cells.

Another proxy for sensing the DL is the ubiquitination of lysosomal proteins.[27] The proteome of patient fibroblasts indicated dysregulated expression of several ubiquitination-related proteins, including UBR4, suggesting impaired recruitment. UBR4, a binding partner of ZFTRAF1, facilitates ubiquitination and proteasomal degradation of short-lived proteins, including N-end rule substrates.[29] Previously, *Ubr4*-deficient mouse embryos have been reported with multiple abnormalities of neurogenesis.[30] We also observed downregulation of UBE2E1, an E2 ubiquitin-conjugating enzyme, which performs degradative ubiquitination,[31] plausibly leading to proteasomal degradation defects in our affected individual. It may be augmented by the combined dysregulated expression of 3 other proteins of deubiquitination, UPS48, UPS10, and UPS24,[32] in our patient fibroblasts.

After lysosomal proteins are ubiquitinated, Gal3 further recruits initiation factors of the autophagic machinery, including ATG16L1 and ATG9A,[33] to start the phagophore formation, and another protein, LC3β binds directly on the expanding phagophore.[27] Our patients' fibroblasts showed considerably reduced ATG16L1, whereas increased amount of LC3β is observed. The former was also validated by the proteome data of the affected individual, thus indicating deleterious mutational effects on the function of autophagic machinery. Inhibition or deletion of autophagy initiation factors is already known to halt phagophores formation, resulting in the accumulation of autophagy substrates, such as p62.[34] Interestingly, DAP1, the most highly upregulated protein in patient-derived fibroblasts, is an essential negative

regulator of autophagy.[35] Similarly, another upregulated protein, MTMRD, also plays a crucial role in autophagy.[36] Their differential expression may also hint at impaired autophagy. Finally, the shrinkage of nuclear size in our patient-derived primary fibroblasts may also depict abnormal autophagy, resulting in cell size reduction and, eventually, cell death.

Our transcriptome data also support the enrichment of DEGs involved in mRNA processing and autophagy in patient-derived fibroblasts. *GATA1* is a highly upregulated transcript with a prominent role in regulating genes necessary for lysosomal function.[19] Similarly, differential expression of *HOXC11* may also hint at impaired autophagy because homeobox (HOX) proteins are also reported to regulate autophagy.[37] Interestingly, we also found differential expression of HOX proteins (HOXB13, HOXC10, HOXC-AS2, HOXC-AS3, HOXC-AS3, and HOXD4) in our proteome data. Moreover, knockout mouse models of *Vangl2* showed elevated level of LAMP-2A and an increased number of chaperone-mediated autophagy lysosomes.[21] Revealing several differentially spliced genes and detecting several alternative splicing events in both affected members may hint at the crucial role of *ZFTRAF1* in mRNA processing. Furthermore, the localization of ZFTRAF1 in nuclear speckles strengthens its essential function in mRNA processing.

Because we could not reprogram the patient fibroblasts into iPSCs, we may attribute it to impaired autophagy, which is crucial for reprogramming fibroblasts into iPSCs. It is in line with a previous study demonstrating impaired reprogramming of fibroblasts into iPSCs due to the depletion of critical autophagy factors in fibroblasts.[34] Furthermore, the inability of iPSCs reprogramming from patient-derived primary fibroblasts could also be attributed to some additional factors that need further investigation.

In conclusion, we have characterized a previously uncharacterized novel protein, ZFTRAF1, and shown the consequence of its dysfunction in human neurodevelopment by dissecting the pathomechanism through multiple complementary strategies. Our findings implicate ZFTRAF1 as a presumable mediator of the autophagic mechanism and mRNA processing. Irregularities in the protein degradation machinery may lead to observed health consequences. However, the role of ZFTRAF1 in both of these processes needs further validation.

Data Availability

The authors submitted the investigated variants of *ZFTRAF1* to ClinVar with the accession numbers SCV003852653, SCV003852700, and SCV003852657. RNA-seq and mass spectrometry proteomics data have been submitted to Gene Expression Omnibus (GEO) and ProteomeXchange Consortium via the PRIDE with accession numbers GSE228834 and PXD044735, respectively. Any of the remaining data of this study could be requested from the corresponding author (mhussain@uni-koeln.de).

Acknowledgments

The authors are grateful to the participating families. For technical help, the authors thank Nina Dalibor from Cologne Center for Genomics, University of Cologne. The authors thank CECAD, University of Cologne, for its mass spectrometry services.

Funding

Funding for this research was obtained from the Center for Molecular Medicine Cologne (Projects 38-RP and C12; 2635/8029/01 and 2635/8326/01) to P.N. and M.S.H.; the Koeln Fortune Program (Faculty of Medicine, University of Cologne; 381/2020) to M.S.H.; Hertie Foundation (P1230037) to M.W.; and DFG Research Unit (FOR2625) to A.S.

Author Information

Conception and Design: M.A., M.S.H.; Funding Acquisition: M.S.H., P.N.; Data Curation: M.A., T.G., B.B., C.B., H.T., K.B., D.W., H.G.M., F.K., I.K., M.W., M.S.H.; Formal Analysis: M.A., A.I.A.K., S.A., U.A., A.S., T.G., J.H., B.B., C.B., H.T., S.M.B., M.I.-G., H.-M.P., M.H., K.B., D.W., H.G.M., F.K., I.K., M.W., M.S.H.; Investigation: M.A., A.I.A.K., A.S., T.G., B.B., H.T., D.W., H.G.M., M.W., M.S.H.; Methodology: M.A., A.I.A.K., S.A., A.S., C.B.; Supervision: P.N., M.S.H.; Writing-original draft: M.A., M.S.H.; Writing-review and editing: M.A., U.A., M.W., P.N., M.S.H.

Ethics Declaration

The Faculty of Medicine and Health Sciences, University of Aden, Yemen, and the Ethics Committee of Pir Mehr Ali Shah Arid Agriculture University Rawalpindi (PMAS-AAUR), Pakistan, approved the study. Participants in the study granted permission, in their local languages, for their photos to be used in the final publication.

Conflict of Interest

The authors declare no conflicts of interest.

Additional Information

The online version of this article (https://doi.org/10.1016/j.gim.2024.101143) contains supplementary material, which is available to authorized users.

Affiliations

[1]Cologne Center for Genomics (CCG), University of Cologne, Faculty of Medicine and University Hospital Cologne, Cologne, Germany; [2]Center for Molecular Medicine Cologne (CMMC), University of Cologne, Faculty of Medicine and University Hospital Cologne, Cologne, Germany; [3]Biochemistry Department, King Saud University, Riyadh, Saudi Arabia; [4]GenAlive Lab, Riyadh, Saudi Arabia; [5]University Institute of Biochemistry and Biotechnology (UIBB), PMAS-Arid Agriculture University Rawalpindi, Rawalpindi, Pakistan; [6]Institute for Biochemistry and Molecular Biology, Medical Faculty, University of Bonn, Bonn, Germany; [7]Cologne Excellence Cluster on Cellular Stress Responses in Aging-Associated Diseases (CECAD), University of Cologne, Cologne, Germany; [8]Department of Paediatric Neurology and Developmental Medicine, Dr. von Hauner Children's Hospital, LMU Hospital Munich, Ludwig-Maximilians-Universität, Munich, Germany; [9]Department of Biological and Biomedical Sciences, The Aga Khan University, Karachi, Pakistan; [10]Health Services Academy (HSA), Ministry of National Health Services Regulations and Coordination (MNHSR&C), Islamabad, Pakistan; [11]Reference Unit for Rare Diseases DiERCyL, Clinical Biochemistry Department, University Hospital of Salamanca, Medicine Department, University of Salamanca, IBSAL, Salamanca, Spain; [12]Institute of Zoology, Developmental Biology Unit, University of Cologne, Cologne, Germany; [13]Department of Neurosurgery, Medical Faculty and University Hospital Düsseldorf, Heinrich-Heine-Universität Düsseldorf, Düsseldorf, Germany; [14]Institute for Human Genetics and Genomic Medicine, Medical Faculty, RWTH Aachen University, Aachen, Germany; [15]Departamento de Pediatría, Hospital Universitario de Salamanca, INCYL member, Salamanca, Spain; [16]Institute of Human Genetics, TUM School of Medicine and Health, Technical University of Munich, Munich, Germany; [17]Institute for Neurogenomics, Helmholtz Zentrum München, Neuherberg, Germany

References

1. Bertacchi M, Tocco C, Schaaf CP, Studer M. Pathophysiological heterogeneity of the BBSOA neurodevelopmental syndrome. *Cells*. 2022;11(8):1260. http://doi.org/10.3390/cells11081260
2. Seki N, Ohira M, Nagase T, et al. Characterization of cDNA clones in size-fractionated cDNA libraries from human brain. *DNA Res*. 1997;4(5):345-349. http://doi.org/10.1093/dnares/4.5.345
3. Menon RP, Strom M, Hughes RC. Interaction of a novel cysteine and histidine-rich cytoplasmic protein with galectin-3 in a carbohydrate-independent manner. *FEBS Lett*. 2000;470(3):227-231. http://doi.org/10.1016/s0014-5793(00)01310-7
4. Bawumia S, Barboni EA, Menon RP, Hughes RC. Specificity of interactions of galectin-3 with Chrp, a cysteine- and histidine-rich cytoplasmic protein. *Biochimie*. 2003;85(1-2):189-194. http://doi.org/10.1016/s0300-9084(03)00007-5
5. Ly-Huynh JD, Lieu KG, Major AT, et al. Importin alpha2-interacting proteins with nuclear roles during mammalian spermatogenesis. *Biol Reprod*. 2011;85(6):1191-1202. http://doi.org/10.1095/biolreprod.111.091686
6. Chen F, Zhang Y, Creighton CJ. Systematic identification of non-coding somatic single nucleotide variants associated with altered transcription and DNA methylation in adult and pediatric cancers. *NAR Cancer*. 2021;3(1):zcab001. http://doi.org/10.1093/narcan/zcab001
7. Rasool S, Baig JM, Moawia A, et al. An update of pathogenic variants in ASPM, WDR62, CDK5RAP2, STIL, CENPJ, and CEP135 underlying autosomal recessive primary microcephaly in 32 consanguineous families from Pakistan. *Mol Genet Genomic Med*. 2020;8(9):e1408. http://doi.org/10.1002/mgg3.1408
8. Brunet T, Jech R, Brugger M, et al. De novo variants in neurodevelopmental disorders-experiences from a tertiary care center. *Clin Genet*. 2021;100(1):14-28. http://doi.org/10.1111/cge.13946
9. Hussain MS, Baig SM, Neumann S, et al. CDK6 associates with the centrosome during mitosis and is mutated in a large Pakistani family with primary microcephaly. *Hum Mol Genet*. 2013;22(25):5199-5214. http://doi.org/10.1093/hmg/ddt374
10. Makhdoom EUH, Waseem SS, Iqbal M, et al. Modifier genes in microcephaly: a report on WDR62, CEP63, RAD50 and PCNT variants exacerbating disease caused by biallelic mutations of ASPM and CENPJ. *Genes*. 2021;12(5):731. http://doi.org/10.3390/genes12050731
11. Hussain MS, Baig SM, Neumann S, et al. A truncating mutation of CEP135 causes primary microcephaly and disturbed centrosomal function. *Am J Hum Genet*. 2012;90(5):871-878. http://doi.org/10.1016/j.ajhg.2012.03.016
12. Asif M, Kaygusuz E, Shinawi M, et al. De novo variants of CSNK2B cause a new intellectual disability-craniodigital syndrome by disrupting the canonical Wnt signaling pathway. *HGG Adv*. 2022;3(3):100111. http://doi.org/10.1016/j.xhgg.2022.100111
13. Mosen P, Sanner A, Singh J, Winter D. Targeted quantification of the lysosomal proteome in complex samples. *Proteomes*. 2021;9(1):4. http://doi.org/10.3390/proteomes9010004
14. Akter F, Bonini S, Ponnaiyan S, et al. Multi–cell line analysis of lysosomal proteomes reveals unique features and novel lysosomal proteins. *Mol Cell Proteomics*. 2023;22(3):100509. http://doi.org/10.1016/j.mcpro.2023.100509
15. Dufour W, Alawbathani S, Jourdain AS, et al. Monoallelic and biallelic variants in LEF1 are associated with a new syndrome combining ectodermal dysplasia and limb malformations caused by altered WNT signaling. *Genet Med*. 2022;24(8):1708-1721. http://doi.org/10.1016/j.gim.2022.04.022
16. Theobald SJ, Simonis A, Georgomanolis T, et al. Long-lived macrophage reprogramming drives spike protein-mediated inflammasome activation in COVID-19. *EMBO Mol Med*. 2021;13(8):e14150. http://doi.org/10.15252/emmm.202114150
17. Tang AD, Soulette CM, van Baren MJ, et al. Full-length transcript characterization of SF3B1 mutation in chronic lymphocytic leukemia reveals downregulation of retained introns. *Nat Commun*. 2020;11(1):1438. http://doi.org/10.1038/s41467-020-15171-6
18. Sobreira N, Schiettecatte F, Valle D, Hamosh A. GeneMatcher: a matching tool for connecting investigators with an interest in the same gene. *Hum Mutat*. 2015;36(10):928-930. http://doi.org/10.1002/humu.22844
19. Kang YA, Sanalkumar R, O'geen H, et al. Autophagy driven by a master regulator of hematopoiesis. *Mol Cell Biol*. 2012;32(1):226-239. http://doi.org/10.1128/MCB.06166-11

20. Cost NG, Czyzyk-Krzeska MF. Regulation of autophagy by two products of one gene: TRPM3 and miR-204. *Mol Cell Oncol*. 2015;2(4):e1002712. http://doi.org/10.1080/23723556.2014.1002712
21. Gong Y, Li Z, Zou S, et al. Vangl2 limits chaperone-mediated autophagy to balance osteogenic differentiation in mesenchymal stem cells. *Dev Cell*. 2021;56(14):2103-2120.e9. http://doi.org/10.1016/j.devcel.2021.06.011
22. Wang S, Xia P, Rehm M, Fan Z. Autophagy and cell reprogramming. *Cell Mol Life Sci*. 2015;72(9):1699-1713. http://doi.org/10.1007/s00018-014-1829-3
23. Ghosh R, Vinod V, Symons JD, Boudina S. Protein and mitochondria quality control mechanisms and cardiac aging. *Cells*. 2020;9(4):933. http://doi.org/10.3390/cells9040933
24. Yim WWY, Mizushima N. Lysosome biology in autophagy. *Cell Discov*. 2020;6(1):6. http://doi.org/10.1038/s41421-020-0141-7
25. Otomo T, Yoshimori T. Lysophagy: a method for monitoring lysosomal rupture followed by autophagy-dependent recovery. *Methods Mol Biol*. 2017;1594:141-149. http://doi.org/10.1007/978-1-4939-6934-0_8
26. Maejima I, Takahashi A, Omori H, et al. Autophagy sequesters damaged lysosomes to control lysosomal biogenesis and kidney injury. *EMBO J*. 2013;32(17):2336-2347. http://doi.org/10.1038/emboj.2013.171
27. Papadopoulos C, Meyer H. Detection and clearance of damaged lysosomes by the endo-lysosomal damage response and lysophagy. *Curr Biol*. 2017;27(24):R1330-R1341. http://doi.org/10.1016/j.cub.2017.11.012
28. Aits S, Kricker J, Liu B, et al. Sensitive detection of lysosomal membrane permeabilization by lysosomal galectin puncta assay. *Autophagy*. 2015;11(8):1408-1424. http://doi.org/10.1080/15548627.2015.1063871
29. Tasaki T, Mulder LC, Iwamatsu A, et al. A family of mammalian E3 ubiquitin ligases that contain the UBR box motif and recognize N-degrons. *Mol Cell Biol*. 2005;25(16):7120-7136. http://doi.org/10.1128/MCB.25.16.7120-7136.2005
30. Kim ST, Lee YJ, Tasaki T, et al. The N-recognin UBR4 of the N-end rule pathway is required for neurogenesis and homeostasis of cell surface proteins. *PLoS One*. 2018;13(8):e0202260. http://doi.org/10.1371/journal.pone.0202260
31. Szymanska K, Boldt K, Logan CV, et al. Regulation of canonical Wnt signalling by the ciliopathy protein MKS1 and the E2 ubiquitin-conjugating enzyme UBE2E1. *Elife*. 2022;11:e57593. http://doi.org/10.7554/eLife.57593
32. Pinto-Fernández A, Davis S, Schofield AB, et al. Comprehensive landscape of active deubiquitinating enzymes profiled by advanced chemoproteomics. *Front Chem*. 2019;7:592. http://doi.org/10.3389/fchem.2019.00592
33. Zavodszky E, Vicinanza M, Rubinsztein DC. Biology and trafficking of ATG9 and ATG16L1, two proteins that regulate autophagosome formation. *FEBS Lett*. 2013;587(13):1988-1996. http://doi.org/10.1016/j.febslet.2013.04.025
34. Itakura E, Kishi-Itakura C, Koyama-Honda I, Mizushima N. Structures containing Atg9A and the ULK1 complex independently target depolarized mitochondria at initial stages of Parkin-mediated mitophagy. *J Cell Sci*. 2012;125(6):1488-1499. http://doi.org/10.1242/jcs.094110
35. Koren I, Reem E, Kimchi A. DAP1, a novel substrate of mTOR, negatively regulates autophagy. *Curr Biol*. 2010;20(12):1093-1098. http://doi.org/10.1016/j.cub.2010.04.041
36. Jean S, Cox S, Nassari S, Kiger AA. Starvation-induced MTMR13 and RAB21 activity regulates VAMP8 to promote autophagosome–lysosome fusion. *EMBO Rep*. 2015;16(3):297-311. http://doi.org/10.15252/embr.201439464
37. Banreti A, Hudry B, Sass M, Saurin AJ, Graba Y. Hox proteins mediate developmental and environmental control of autophagy. *Dev Cell*. 2014;28(1):56-69. http://doi.org/10.1016/j.devcel.2013.11.024